

Modeling the propagation characteristics of chorus using CRRES suprathermal electron fluxes

J. Bortnik,¹ R. M. Thorne,¹ and N. P. Meredith²

Received 21 December 2006; revised 17 May 2007; accepted 4 June 2007; published 7 August 2007.

[1] In the present paper, phase space density functions of the form $f(v) = A_N/v^n$ are fitted to statistical distributions of suprathermal electron fluxes ($E = 0.213\text{--}16.5$ keV) from the CRRES satellite, parameterized by L -shell, Magnetic Local Time (MLT), and geomagnetic activity. The fitted distributions are used in conjunction with ray tracing to calculate the Landau damping rates of an ensemble of rays representing whistler-mode chorus waves. The modeled propagation characteristics are compared with observations of chorus wave power from the CRRES satellite, as a function of L -shell, MLT, and magnetic latitude, in various frequency bands, and under various geomagnetic conditions. It is shown that the model results are remarkably consistent with many aspects of the observed wave distributions, including frequency, L -shell, MLT, and latitudinal dependence. In addition, the MLT distribution of wave power becomes characteristically asymmetric during active geomagnetic conditions, with small propagation lengths on the nightside which increase with MLT and maximize on the dayside. This asymmetry is shown to be directly related to the dynamics of the Landau resonant suprathermal electrons which drift around the Earth whilst undergoing scattering and loss due to a variety of plasma waves. Consequently, the suprathermal electrons play an important role in radiation belt dynamics, by controlling the distribution of chorus, which in turn contributes to the acceleration and loss of relativistic electrons in the recovery phase of storms.

Citation: Bortnik, J., R. M. Thorne, and N. P. Meredith (2007), Modeling the propagation characteristics of chorus using CRRES suprathermal electron fluxes, *J. Geophys. Res.*, 112, A08204, doi:10.1029/2006JA012237.

1. Introduction

[2] General description, background, characteristics Chorus emissions are naturally-produced electromagnetic waves in the ELF/VLF ($\sim 0.1\text{--}10$ kHz) frequency range [e.g. reviews by Omura *et al.*, 1991; Sazhin and Hayakawa, 1992] that occur outside the plasmapause predominantly in the dawn sector, and rank among the most intense whistler-mode emissions in the inner magnetosphere [Koops and Roeder, 1990; Meredith *et al.*, 2001; Santolik *et al.*, 2004]. They typically occur in a series of short (~ 0.1 sec), rising tones (though falling and mixed tones are also observed) between $\sim 0.2\text{--}2$ kHz/sec, in two distinct frequency bands that peak in power near $0.34 f_{ce}$ (lower band) and $0.53 f_{ce}$ (upper band), where f_{ce} is the equatorial gyrofrequency along that field-line [Burris and Helliwell, 1969, 1976], and exhibit a wave power minimum near $0.5 f_{ce}$ [Tsurutani and Smith, 1974; Koops and Roeder, 1990]. Chorus intensity and occurrence are directly related to geomagnetic activity [Storey, 1953; Tsurutani and Smith, 1974; Burris and Helliwell, 1976; Meredith *et al.*, 2001, 2003a, 2003b;

Santolik *et al.*, 2003, 2004; Smith *et al.*, 1999, 2004; Spasojevic and Inan, 2005] and it is generally agreed that the generation mechanism involves cyclotron resonance with eastward-drifting, freshly-injected, unstable electron populations in the $\sim 10\text{--}100$ keV range, though the exact generation mechanism remains a topic of intense research [Helliwell, 1967, 1995; Omura *et al.*, 1991; Hattori *et al.*, 1991; Sazhin and Hayakawa, 1992; Trakhtengerts, 1995, 1999; Nunn *et al.*, 1997].

[3] Though chorus has been actively studied for well over 50 years [Storey, 1953], it has recently enjoyed a resurgence of interest due to the recognition of its importance in controlling radiation-belt dynamics [e.g., Horne and Thorne, 1998; Summers *et al.*, 1998, 2004; Horne *et al.*, 2003, 2005a, 2005b; Thorne *et al.*, 2005a, 2005b; Spasojevic and Inan, 2005; Meredith *et al.*, 2002a, 2002b, 2003b; Miyoshi *et al.*, 2003; Lyons *et al.*, 2005; Smith *et al.*, 2004; Varotsou *et al.*, 2005; Shprits *et al.*, 2006] playing a dual role in both the precipitation and acceleration of radiation-belt electrons [Horne and Thorne, 2003; Horne *et al.*, 2005b; Bortnik and Thorne, 2006]. In the scenario described in the above works, lower energy electrons ($\sim 10\text{--}100$ keV) generate chorus near the geomagnetic equator through the loss-cone instability and thermal anisotropy, and scatter these electrons into the loss-cone in the process, resulting in decreased fluxes [*Ibid*]. The locally generated waves also interact with higher energy electrons at large pitch-angles, contributing to the acceleration of electrons to relativistic

¹Department of Atmospheric and Oceanic Sciences, University of California, Los Angeles, California, USA.

²British Antarctic Survey, Natural Environment Research Council, Cambridge, UK.

energies [e.g., *Meredith et al.*, 2002a; *Horne and Thorne*, 2003]. Chorus waves then propagate to higher latitudes, where they resonate with relativistic (MeV) electrons leading to both microburst precipitation, and further acceleration of trapped relativistic electrons [*Horne and Thorne*, 2003; *Horne et al.*, 2005b]. Chorus thus plays a mediating role, transferring energy from the abundant lower energy electron population to the smaller population of higher energy electrons [e.g., *Thorne et al.*, 2005b; *Horne et al.*, 2006]. In order to properly quantify this mediation process, it is important to understand the propagation characteristics of chorus, its wave normal evolution, damping, and resultant distribution of power with respect to latitude, L -shell, and magnetic local time (MLT).

[4] Previous studies have shown that chorus typically occurs between $3 < L < 9$, with a peak at $6 < L < 8$ [*Tsurutani and Smith*, 1974; *Burtis and Helliwell*, 1976; *Meredith et al.*, 2001], in the dawn and afternoon sectors, moving to higher L -shells and/or latitudes when moving towards the day side [*Burtis and Helliwell*, 1976; *Meredith et al.*, 2001]. Wave normal studies show that near the geomagnetic equator, the \mathbf{k} -vector is predominantly field-aligned [*Burton and Holzer*, 1974; *Goldstein and Tsurutani*, 1984] in agreement with theoretical predictions [*Kennel and Thorne*, 1967] but becomes progressively more oblique as it propagates away from the equatorial generation region in a nonducted mode [*Thorne and Kennel*, 1967; *Burton and Holzer*, 1974; *Goldstein and Tsurutani*, 1984]. However, recent observations of chorus, particularly at off-equatorial positions, indicate that generation may have occurred at much higher wave normal angles [*Lauben et al.*, 2002; *Chum and Santolik*, 2005; *Santolik et al.*, 2006]. In both cases, propagation is found to be away from the equatorial region [*LeDocq et al.*, 1998; *Lauben et al.*, 2002; *Santolik et al.*, 2004, 2005], with very few exceptions where weak magnetospheric reflections have been observed [*Maeda and Smith*, 1981; *Parrot et al.*, 2003, 2004]. There is strong support for the fact that propagation is predominantly nonducted [e.g., *Burton and Holzer*, 1974; *Goldstein and Tsurutani*, 1984; *Lauben et al.*, 2002; *Chum and Santolik*, 2005] and apparently limited by Landau damping [*Bortnik et al.*, 2006] to propagation ranges of 10° – 20° in latitude [*Burtis and Helliwell*, 1976; *Meredith et al.*, 2001].

[5] The relation of chorus morphology to the storm-time injection and dispersive (eastward) azimuthal drift of energetic electrons has been well-noted by past workers [*Anderson and Maeda*, 1977; *Collier and Hughes*, 2004a, 2004b; *Smith et al.*, 2004; *Abel et al.*, 2006; *Lubchich et al.*, 2006], where the electrons were treated as the source of the chorus waves. In the present work, we neglect all aspects of the wave generation process, and consider only the (linear) Landau damping of the chorus waves as they propagate in an unducted mode away from their source region. Specifically, we examine the effects of suprathermal electron fluxes upon chorus propagation characteristics using a combination of measured fluxes, ray tracing, and comparison to wave data. In section 2, statistical averages of suprathermal fluxes from the CRRES satellite are presented, parameterized by MLT, L -shell, and geomagnetic activity (section 2.1), and analytical phase space density functions are fitted to these measurements (section 2.2). In section 3 the ray tracing and Landau damping methodology is pre-

sented using a single ray (section 3.1), and the results of ray tracing a large distribution of rays are shown (section 3.2). The ray tracing results are compared to chorus wave measurements made on the CRRES satellite in section 4, in terms of geomagnetic activity dependence (section 4.1) and frequency dependence (section 4.2), and the agreement and limitations of our model are discussed in section 5. The major findings of this work are summarized in section 6.

2. The CRRES Satellite and Database

[6] The Combined Release and Radiation Effects Satellite (CRRES) [*Johnson and Kierein*, 1992] is particularly well-suited for the present study due to its favorable orbit and instrumentation suite, and is used to provide information on the suprathermal electron fluxes, as well as chorus wave intensities (discussed further in section 4). The spacecraft was launched on July 25, 1990 and operated in a highly elliptical geosynchronous transfer orbit with a perigee of 305 km, an apogee of 35,768 km, and an inclination of 18° . The orbital period was approximately 10 hours, and the initial apogee was at a magnetic local time (MLT) of 0800 MLT. The magnetic local time of apogee decreased at a rate of approximately 1.3 hours per month until the satellite failed on October 11, 1991, when the apogee was at approximately 1400 MLT. The satellite swept through the most important chorus source region approximately 5 times per day, providing coverage for almost 15 months.

[7] The suprathermal electron fluxes were measured by the Low Energy Plasma Analyzer (LEPA). This instrument consisted of two electrostatic analyzers with microchannel plate detectors, each with a field of view of $120^\circ \times 5^\circ$, one measuring electrons and the other ions in the energy range $100 \text{ eV} < E < 30 \text{ keV}$ [*Hardy et al.*, 1993]. The instrument detected the complete pitch angle range from 0° to 180° every 30 sec with a resolution of $5.625^\circ \times 8^\circ$ at 20 energy channels in the range $100 \text{ eV} < E < 30 \text{ keV}$. The chorus waves were measured by the Plasma Wave Experiment (PWE) which detected the wave electric field from 5.6 Hz to 400 kHz, using a 100-m tip-to-tip long wire antenna, with a dynamic range covering a factor of at least 10^5 in amplitude [*Anderson et al.*, 1992].

[8] In order to examine the global morphology of the suprathermal electron fluxes and the chorus wave intensities as a function of geomagnetic activity we constructed a database from the CRRES wave and particle observations. The wave data were initially corrected for the instrumental background response and smoothed by using a running 3-min average to take out the beating effects due to differences in the sampling and the spin rate. Spurious data points, data spikes, and periods of instrumental downtime were flagged and ignored in the subsequent statistical analyses. Twelve orbits, during which nontraditional configurations were deployed for testing purposes, were also excluded from the analyses.

[9] The electric field intensities, discussed in section 4, together with the electron perpendicular differential number flux for each energy level of the LEPA instrument were then rebinned as a function of half orbit (outbound and inbound) and L in steps of 0.1 L . The data were recorded together with the universal time (UT), magnetic latitude (λ_m), magnetic local time (MLT), the AE index, and time spent

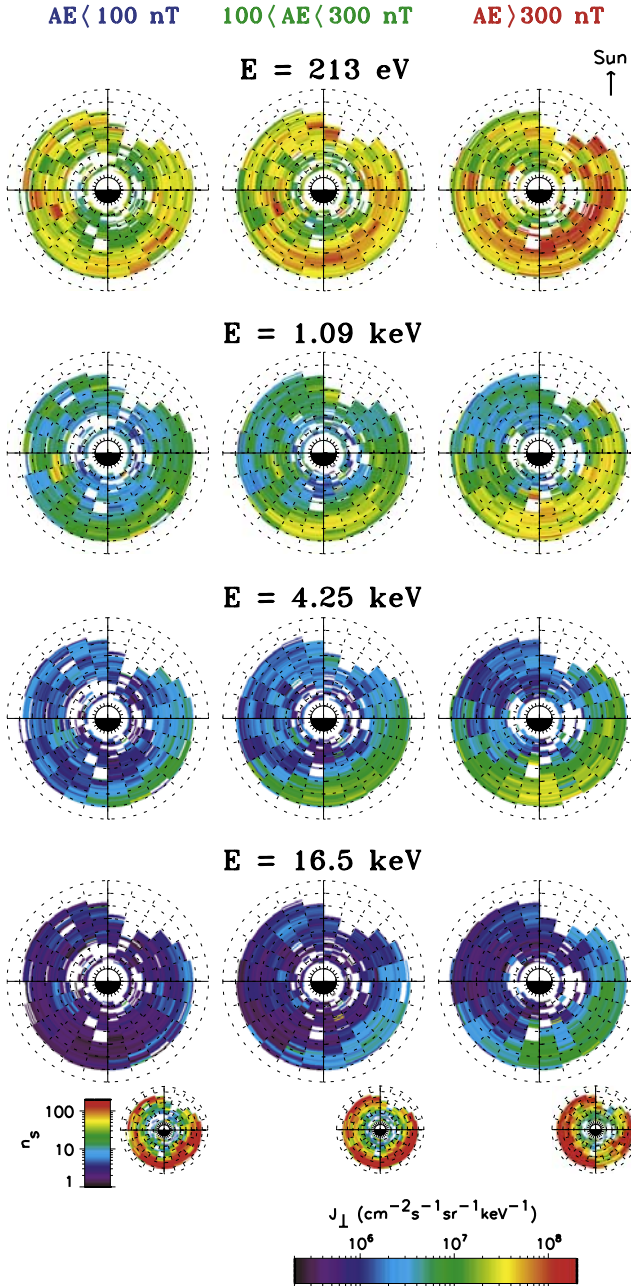


Figure 1. Average suprathermal electron fluxes measured with the LEPA instrument on the CRRES satellite. Distributions are shown as a function of L -shell and MLT, parameterized by energy (rows: 0.213, 1.09, 4.25, and 16.5 keV), and magnetic activity levels (columns: $\text{AE} < 100 \text{ nT}$, $100 < \text{AE} < 300 \text{ nT}$, and $\text{AE} > 300 \text{ nT}$). The common colorbar is shown at the bottom of the figure, together with the number of samples in each L -MLT bin.

in each bin with the same resolution. The resulting database, consisting of plasma wave and particle measurements from 939 orbits (1878 half orbits), was subsequently analyzed to determine the behavior of the waves and the particles as a function of spatial location and magnetic activity.

[10] Both whistler mode chorus and the suprathermal electrons tend to be observed outside of the plasmapause.

In order to exclude wave emissions and electron fluxes from inside the plasmapause from the survey we adopt a criterion based on the amplitude of the waves in the band $f_{ce} < f < 2f_{ce}$ following [Meredith *et al.*, 2004]. Waves in this frequency band, which contain contributions from both electron cyclotron harmonic waves and thermal noise, tend to be excluded from the high density region inside the plasmapause, and have proven to be an excellent indicator of times when the satellite is outside the plasmapause. The specific criterion we adopt, based on a previous experimental study using data from the CRRES Plasma Wave Experiment, requires that the wave amplitude for frequencies in the range $f_{ce} < f < 2f_{ce}$ be greater than 0.0005 mVm^{-1} in order for the wave and particle data to be included in the survey [Meredith *et al.*, 2004].

2.1. Suprathermal Flux Observations

[11] Figure 1 shows the average distribution of perpendicular suprathermal electron fluxes measured with LEPA on the CRRES satellite, averaged over a range of magnetic latitudes within $\pm 15^\circ$ of the magnetic equator. Each panel displays fluxes in color as a function of L -shell and MLT, with the common colorbar shown at the bottom of the figure. The fluxes are parameterized by energy channel and geomagnetic activity, showing (rows from top to bottom) the 0.213 eV, 1.09 keV, 4.25 keV and 16.5 keV channels, for the magnetic activity conditions (columns from left to right) $\text{AE} < 100 \text{ nT}$, $100 < \text{AE} < 300 \text{ nT}$, and $\text{AE} > 300 \text{ nT}$. The statistical coverage of CRRES is shown at the bottom of each column, as the number of samples in each L -MLT bin. These specific energy channels have been chosen for a number of reasons: firstly, the range 0.213–16.5 keV was chosen because the suprathermal electron energies responsible for Landau damping of chorus waves fall comfortably within it, typically near $\sim 1 \text{ keV}$ [e.g., Bortnik and Thorne, 2006, Figure 3d]. Secondly, the choice of using only four of the energy channels available on CRRES was made because it is the smallest number of points that gives a robust parameter fit (discussed further below) and adding more data has little or no further effect upon the fitted distribution, but only increases computation length. The spacing of energy channels was chosen to be roughly even on a logarithmic scale, in both energy and velocity space (see for example Figure 2).

[12] The flux distributions show that suprathermal fluxes at all energies increase with increasing geomagnetic activity, and penetrate to lower L -shells, due to the enhanced convection electric field [e.g., Korth *et al.*, 1999]. The MLT distributions also become more asymmetric with increasing geomagnetic activity, due to increases in both electron injection, and loss as they drift eastward around the Earth. Low energy ($< 16 \text{ keV}$) electrons are subject to strong diffusion loss during resonance with electrostatic electron cyclotron harmonic (ECH) waves [Horne and Thorne, 2000] and whistler-mode chorus [Glauert and Horne, 2005]. The loss timescale for strong diffusion is considerably shorter than the drift timescale at these energies, giving rise to strong MLT gradients.

[13] It should be noted that a few L -MLT bins do not contain particle data due to incomplete coverage by CRRES (e.g., $4 < L < 5$, $2300 < \text{MLT} < 0000$, and $L > 6$ at $0900 < \text{MLT} < 1200$). While we have taken measures to avoid most

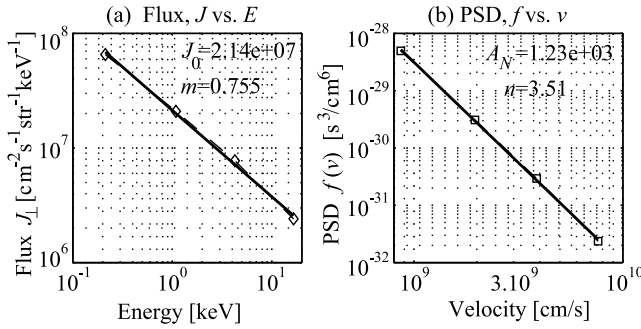


Figure 2. Analytical fits to (a) flux values at 4 energies, and transformed into (b) phase space density (PSD) as a function of velocity, at $L = 4.45$, MLT = 5.5, and AE > 300 nT.

regions with insufficient coverage, for example only considering the region $3 < L < 7$ in subsequent analysis, a few such regions still remain. This problem has been addressed by smoothing and interpolating the data in logarithmic space over the 2D plane. A number of different techniques of data filling have been compared including more elaborate techniques [Kondrashov and Ghil, 2006], but since our data set is fairly smooth (particularly when the logarithm is used for interpolation), the results obtained using the various methods agreed fairly well, and a simple triangle interpolation scheme, using a gradient regularizer was chosen.

2.2. Parameter Fitting

[14] We aim to fit analytical functions representing the phase space density as a function of velocity, $f(v)$, to the suprathermal flux observations shown in Figure 1, at every L , and MLT bin. The fitted $f(v)$ functions can subsequently be used to calculate Landau damping rates when combined with ray tracing. In order to illustrate our methodology, a specific location is chosen, e.g., $L = 4.45$, MLT = 5.5, together with a geomagnetic activity level, e.g., AE > 300 nT, giving the 4 measured flux values (J_{1-4}) corresponding to the 4 energy channels ($E_{1-4} = 0.213, 1.09, 4.25$, and 16.5 keV), illustrated as the diamond symbols in Figure 2a. If an assumed distribution of the form:

$$J(E) = \frac{J_0}{E^m} \quad (1)$$

is used, the J_0 and m values can be readily obtained by taking the logarithm of equation (1)

$$\underbrace{\log_{10}(J_i)}_{y_i} = \underbrace{\log_{10}(J_0)}_{a_0} - \underbrace{m}_{a_1} \underbrace{\log_{10}(E_i)}_{x_i} \quad (2)$$

and solving for a_0 , a_1 in equation (2) in a least-squares sense [Press et al., 2002, p.661] where (E_i, J_i) or (x_i, y_i) , $i = 1 - 4$, are the data points. The overall goodness of fit is estimated by the sum of squared residuals between the fitted curve and actual data points. The least-squares fit described above is shown in Figure 2a as the solid, heavy line, with the fit-parameters $J_0 = 2.14 \times 10^7 \text{ cm}^{-2} \text{ sec}^{-1} \text{ str}^{-1} \text{ keV}^{-1}$, and $m = 0.755$. For comparison, the data points are joined with

a dashed line in Figure 2a, showing that the agreement between data and fitted model is very good.

[15] The flux $J(E)$ can be related to the phase space density $f(v)$ through the simple non-relativistic relation [Walt, 1994, p. 67]:

$$J(E) = \frac{v^2}{m'} f(v) \quad (3)$$

where v and m' are the electron velocity and mass respectively, but care must be exercised with regard to the selection of units. If the energy E is given in keV, and v in cm^{-1} as is conventionally done in cgs units, then:

$$m' = \kappa_0 m_e \quad (4)$$

where $m_e = 9.1 \times 10^{-31} \text{ kg}$, and $\kappa_0 = 6.25 \times 10^{11} \text{ C}^{-1}$ is a unit correction factor. Using equations (3) and (4) we can translate the flux data points (J_i, E_i) to phase space density data points (v_i, f_i) as shown by the square symbols in Figure 2b.

[16] If we further assume the phase space density expression to be of the form:

$$f(v) = \frac{A_N}{v^n} \quad (5)$$

as has been done previously [Bell et al., 2002], then combining equations (1)–(5) gives:

$$n = 2a_1 + 2 \quad (6)$$

$$A_N = \frac{2 \times 10^{a_0}}{\left(\frac{1}{2} m'\right)^{a_1-1}} \quad (7)$$

[17] We show in Figure 2b the fitted distribution of Figure 2a, translated to a phase space density function $f(v)$ in the form equation (5), with the fit parameters $n = 3.51$ and $A_N = 1.23 \times 10^3 \text{ s}^3 \text{ cm}^{-6}$, where the data points are again joined by a dashed line which is completely obscured by the fitted distribution, indicating an excellent fit.

[18] It should also be mentioned that we experimented with a phase space density of the form $f(v) = A_N / (v^2 + v_0^2)^{n/2}$, and fitted to the data points using a simulated annealing algorithm [Kirkpatrick et al., 1983], but in all cases the thermal velocity v_0 was found to be negligible, so the simpler form equation (2) was used instead and fitted with the computationally economical least-squares method.

3. Ray Tracing and Landau Damping

[19] The fitted distribution discussed in Section 2.2 can now be combined with ray tracing to study the propagation characteristics of chorus. We use the same methodology as Bortnik et al. [2006], which is illustrated in Figure 3.

3.1. Ray Tracing Methodology

[20] Using the Stanford VLF raytracer [Inan and Bell, 1977], individual rays representative of chorus waves are injected at the magnetic equatorial plane ($\lambda = 0^\circ$), with an initial wave normal angle $\psi = 0^\circ$, at a given L -shell, MLT,

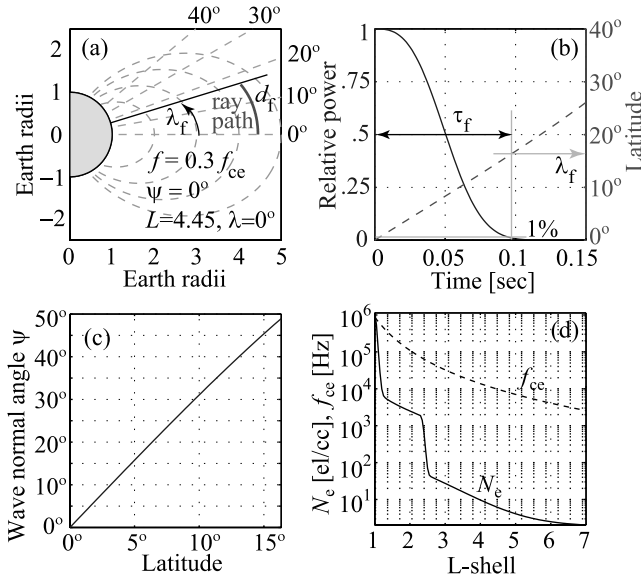


Figure 3. Illustration of ray propagation at $L = 4.45$, $\text{MLT} = 5.5$, $\psi = 0^\circ$, $f = 0.3 f_{\text{ce}}$ and $\text{AE} > 300 \text{ nT}$. (a) ray path shown in heavy line, with final latitude λ_f , and propagation distance d_f indicated; (b) relative wave power (solid line) and ray latitude (dashed line) as a function of group time, showing the 1% power level which defines ray termination, giving $\tau_f = 0.0971 \text{ sec}$, $\lambda_f = 16.34^\circ$, and $d_f = 1.28 R_E$; (c) wave normal angle evolution as a function of ray latitude, and (d) equatorial electron number density used in all simulations, and electron gyrofrequency f_{ce} as a function of L -shell.

and frequency f which is normalized to the equatorial gyrofrequency f_{ce} . For example, Figure 3a shows the propagation of a single ray in the meridional plane, injected at $L = 4.45$, $\lambda = 0^\circ$, $\psi = 0^\circ$, and $f = 0.3 f_{\text{ce}}$. In the course of the ray propagation, the appropriate suprathermal distribution $f(v)$ is used to calculate the Landau damping rate at every point along the ray path [Brinca, 1972; Bortnik et al., 2003], and integrated to give the total damping of the ray. Figure 3b shows the total damping calculated for the ray in panel (a), using the corresponding distribution illustrated in Figure 2b (solid line) as a function of group time, together with the latitude of the ray (dashed line). The point where the ray power reaches 1% of its initial value is considered to be the termination of the wave, and the corresponding final time τ_f and final latitude λ_f are indicated on the figure. In the present case shown in Figure 3b, $\tau_f = 0.0971 \text{ sec}$, $\lambda_f = 16.34^\circ$, and in Figure 3a the ray path is only shown until the termination point, also indicating the final propagation distance $d_f = 1.28 R_E$.

[21] We note that since we only have comprehensive information on perpendicular suprathermal fluxes (Figure 1), the pitch-angle distribution is not known for all cases, so it is assumed to be isotropic for simplicity. This assumption is consistent with past work which has indicated that suprathermal fluxes are generally isotropic [Bell et al., 2002], and even if some anisotropy is present, it does not affect the Landau damping rates appreciably [Thorne and Horne, 1994]. The assumption of suprathermal flux isotropy is particularly valid during active times (which are of most

interest to us in the present study) when the presence of intense waves tends to isotropise the electron distribution [Asnes et al., 2005] at lower energies.

[22] In Figure 3c, the wave normal angle of the ray is shown as a function of latitude, to the point of termination at $\lambda_f = 16.34^\circ$. Even though the ray propagates for a relatively short distance, it should be noted that the wave normal angle rotates to relatively high values $\psi \sim 50^\circ$ in the course of its lifetime, which accelerate its damping (c.f. Figure 3b) [Brinca, 1972; Thorne and Horne, 1994].

[23] We note that in Figure 3, and all subsequent ray tracing simulations in the present study, the \mathbf{B} -field model was assumed to be a simple dipole, and the equatorial gyrofrequency f_{ce} is shown as the dashed line in Figure 3d. The equatorial number density was modeled after Carpenter and Anderson [1992], with the plasmapause set at $L_{\text{pp}} \sim 2.5$ corresponding to geomagnetic activity levels with $K_p^{\max} \sim 6.7$ (maximum value of K_p in the preceding 24 hours). Off-equatorial values were calculated using the diffusive equilibrium model [Angerami and Thomas, 1964].

3.2. Calculation Results

[24] The single ray example illustrated in Figure 3 can be repeated multiple times, in each case varying one of the initial parameters (e.g., L , MLT , AE , f , etc.), and the effect observed in the propagation parameters (e.g., τ_f , λ_f , d_f). The results of this analysis are shown in Figure 4, where the final latitude λ_f of each ray is plotted as a function of its initial L -shell and MLT , parameterized into 3 columns representing geomagnetic activity (corresponding to Figure 1), and 4 rows corresponding to the ray frequency normalized to the equatorial gyrofrequency (please note the color-bar is different for each row). The frequencies have been chosen to represent chorus rays ranging from the lowest observed values (row A, $f = 0.1 f_{\text{ce}}$), through typical lower band (row B, $f = 0.3 f_{\text{ce}}$) and upper band (row C, $f = 0.5 f_{\text{ce}}$), to the highest observed frequencies (row D, $f = 0.7 f_{\text{ce}}$). The initial wave normal angle was set to $\psi = 0^\circ$ in all the simulations. The values at $L \sim 5-7$, $\text{MLT} \sim 0900-1200$ (indicated by the dashed oval in panel (Ab)) should be interpreted with caution since this region corresponds to interpolated fluxes (c.f. Figure 1, Section 2.1). The dark blue regions appearing at low L -shells in panels (Aa) and (Ac), $\text{MLT} = 1600$ and 0600 respectively, correspond to rays that are able to undergo a magnetospheric reflection [e.g., Parrot et al., 2003, 2004; Bortnik et al., 2006] and return to low latitudes before being extinguished, due to the very low damping (corresponding to low frequency of the wave) and low L -shell, as discussed further below. Since our density profile was fixed in all simulations (e.g. Figure 3d), the expected average location of the plasmapause L_{pp} was marked explicitly in columns a and b, with $L_{\text{pp}} \sim 5.1$ corresponding to $K_p^{\max} \sim 1$ in column a, $L_{\text{pp}} \sim 3.75$ corresponding to $K_p^{\max} \sim 4$ in column b [Carpenter and Anderson, 1992], and $L_{\text{pp}} = 2.5$ in column c as shown in Figure 3d. The chosen K_p^{\max} values are not necessarily proportional to the corresponding AE ranges, but are typical of quiet, moderately disturbed, and disturbed conditions, and are likely to be encountered in the given AE ranges. Since chorus is typically observed outside the plasmapause [e.g., Anderson and Maeda, 1977], only values at $L > L_{\text{pp}}$ should be considered valid in the following discussion.

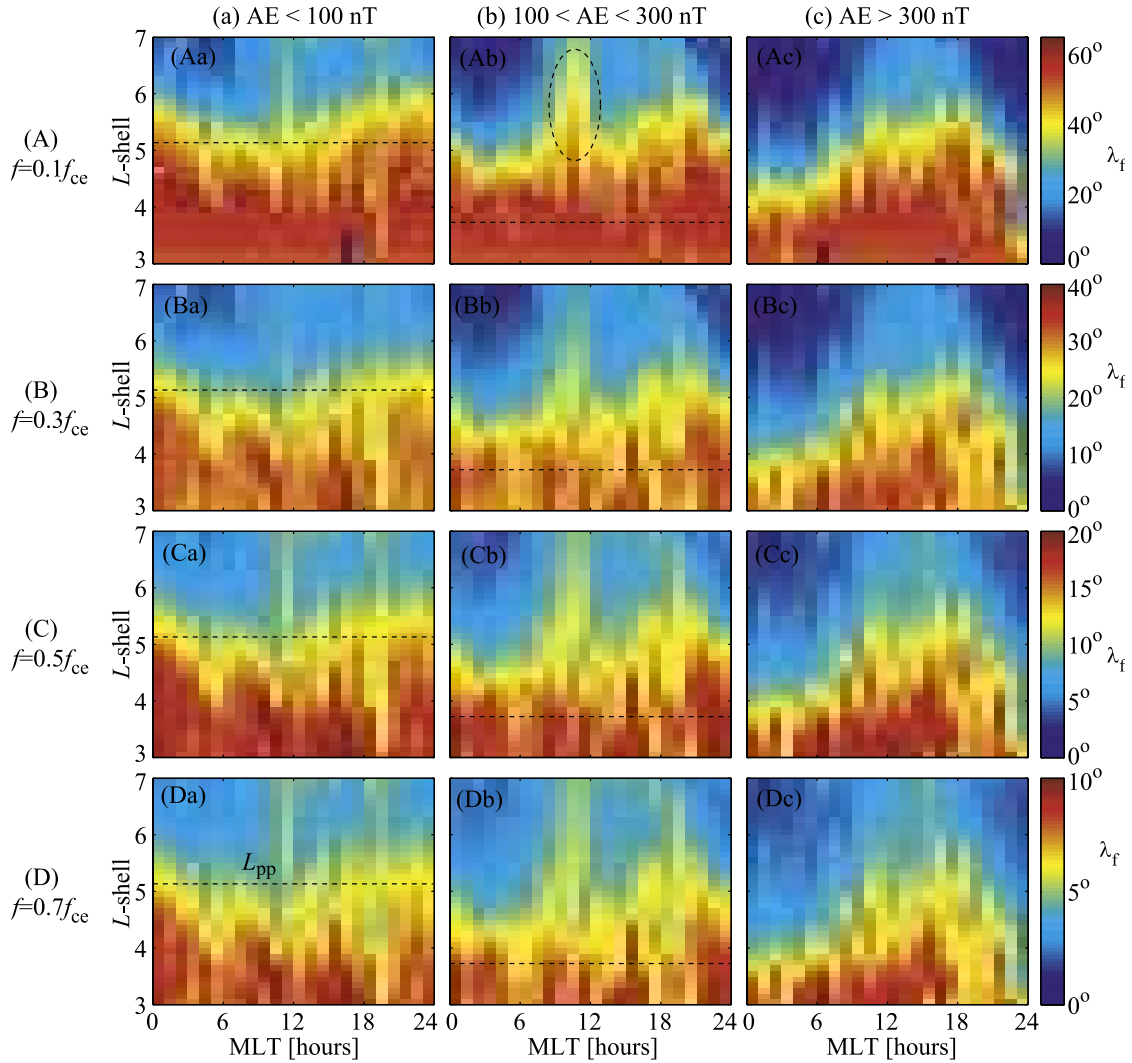


Figure 4. Final propagation latitude λ_f of rays representing chorus, shown as a function of initial L -shell (ordinate) and MLT (abscissa). Rows A–D represent the normalized frequency of each ray ($f/f_{ce} = 0.1, 0.3, 0.5$, and 0.7 respectively) and columns a–c represent geomagnetic activity level as indicated. Horizontal dashed lines indicate an approximate plasmapause L_{pp} location, and the oval region in panel (Ab) should be interpreted with caution since it represents a region of poor satellite coverage (c.f. Figure 1) and consists largely of interpolated flux values.

[25] There are a number of features evident in Figure 4 which we discuss below. Firstly, in each panel it is evident that rays initiated at lower L -shells propagate to higher latitudes than those starting at higher L -shells, regardless of AE or f , for example in panel (Bc), $\lambda_f(L < 4) \sim 30^\circ$ whereas $\lambda_f(L > 6) \sim 10^\circ$. The same behavior (not shown) is also evident for the final propagation distance d_f , confirming that this is a real damping effect is not just a result of longer field-lines at higher L -shells. This behavior is related to the fact that damping rates are proportional to N_h/N_0 [Brinca, 1972], where N_h is the number of ‘hot’ particles, i.e., suprathermal flux, and N_0 is the background cold plasma density. Since convective injection of hot particles into the inner magnetosphere is more efficient at higher L than lower L , and cold plasma density is higher at lower L than at higher L (Figure 3d), the ratio N_h/N_0 is lower at lower L , corresponding to larger λ_f , and vice versa at higher L .

[26] The second feature to note is that in all panels, independent of AE or f , the rays are completely damped while they are still propagating away from the equator, and thus (typically) do not magnetospherically reflect and return to the equator. This unidirectional propagation away from the equator has been well-noted in experimental studies [LeDocq et al., 1998; Lauben et al., 2002; Santolik et al., 2004, 2005], and previously explained on the basis of Landau damping [Bortnik et al., 2006] (though only a single hypothesized suprathermal distribution was used in that case). In the present study, the unidirectional propagation of chorus is confirmed using measured, local flux distributions.

[27] The MLT distribution of λ_f exhibits a distinct progression at all frequencies when geomagnetic activity is increased from quiet times (column a) to disturbed times (column c). For example, examining λ_f at a location of +1

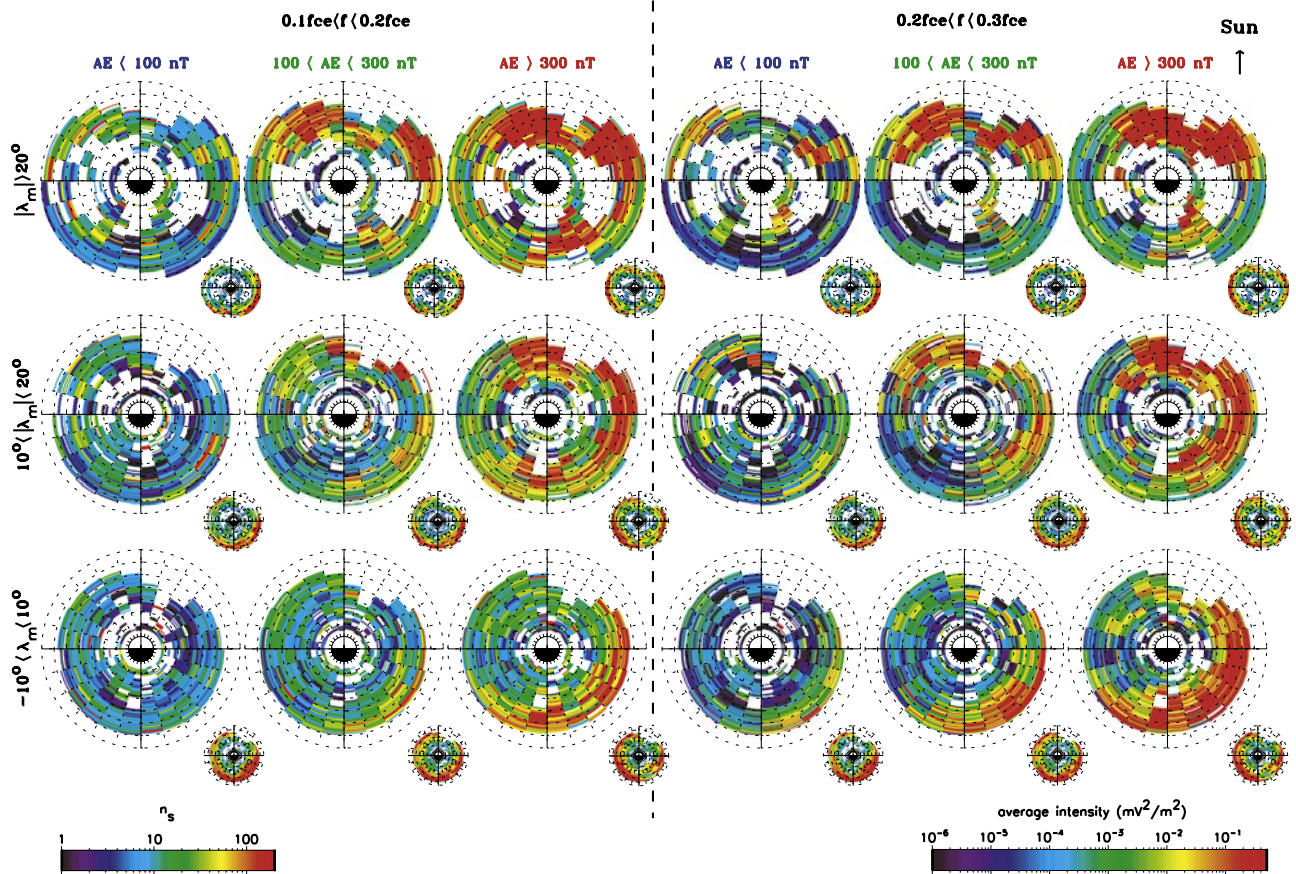


Figure 5. Distribution of chorus wave power as a function of L -shell and MLT, parameterized by magnetic latitude range, rows 1–3: $|\lambda_m| < 10^\circ$, $10^\circ < |\lambda_m| < 20^\circ$, $|\lambda_m| > 20^\circ$; and geomagnetic activity, columns 1–3: $\text{AE} < 100 \text{ nT}$, $100 < \text{AE} < 300 \text{ nT}$, and $\text{AE} > 300 \text{ nT}$. The 9 panels on the left and right correspond to frequency ranges of $0.1 f_{\text{ce}} < f < 0.2 f_{\text{ce}}$ and $0.2 f_{\text{ce}} < f < 0.3 f_{\text{ce}}$ respectively. The colorbars represent average wave intensity and number of samples in each bin.

L -shell outside the plasmapause, in panel (Ba) it is clear that $\lambda_f(L = 6) \sim 15^\circ$ and relatively independent of MLT, with perhaps slightly increased values near midnight. Comparing to panel (Bc), $\lambda_f(L = 3.5, \text{MLT} = 0000) \sim 27^\circ$, and $\lambda_f(L = 3.5, \text{MLT} = 1200) \sim 40^\circ$, there is a pronounced MLT dependence at all L and f , with low values near midnight, increasing with MLT towards noon, peaking postnoon and returning to low values again at night. This geomagnetically controlled MLT dependence is related to the drift and loss timescales of suprathermal electrons which ultimately control the damping of the chorus waves, and will be discussed further in Section 5.

[28] Finally, we note that λ_f is strongly frequency dependent, regardless of AE, MLT or L -shell. Lower frequency components (row A) propagate furthest, with λ_f decreasing as the frequency is increased (e.g., row D). For example, at $L = 4$, $\text{MLT} = 1200$, $\text{AE} > 300 \text{ nT}$, $\lambda_f(f = 0.1 f_{\text{ce}}) \sim 56^\circ$, $\lambda_f(f = 0.3 f_{\text{ce}}) \sim 28^\circ$, $\lambda_f(f = 0.5 f_{\text{ce}}) \sim 15^\circ$, and $\lambda_f(f = 0.7 f_{\text{ce}}) \sim 7.5^\circ$. The tendency of higher frequencies to Landau damp more severely has been previously noted [Thorne and Horne, 1994; Bortnik et al., 2003] in relation to magnetospherically reflected whistler propagation studies, and is due to the combination that (i) higher frequency waves resonate with lower energy electrons which are more abundant (and have larger values of $\partial f / \partial v_{||}$), and (ii) that higher frequency

waves also rotate faster to the resonance cone, which is at lower angles than for lower frequency waves.

4. Comparison to Observations

[29] In order to compare our simulated results to observations we use the CRRES wave data, processed and rebinned as described in Section 2. Only the wave data inferred to be outside the plasmapause are included, by adopting the criterion that the wave amplitude for frequencies in the range $f_{\text{ce}} < f < 2 f_{\text{ce}}$ must be greater than 0.0005 mVm^{-1} [e.g., Meredith et al., 2004]. For the present comparison, the chorus wave intensities were defined by integrals of the averaged wave spectral density ($\text{V}^2 \text{ m}^{-2} \text{ Hz}^{-1}$) over the frequency range $0.1 f_{\text{ce}} < f < 1.0 f_{\text{ce}}$ in steps of $0.1 f_{\text{ce}}$, where f_{ce} is the equatorial electron gyrofrequency as above. The gyrofrequency f_{ce} was determined from the local ambient magnetic field determined from the fluxgate magnetometer instrument [Singer et al., 1992] assuming a dipole field.

4.1. Dependence on Geomagnetic Activity

[30] In Figure 5 we show the chorus wave power binned as a function of L -shell and MLT, parameterized by magnetic latitude range (rows 1–3: $|\lambda_m| > 20^\circ$, $10^\circ < |\lambda_m| < 20^\circ$, $|\lambda_m| < 10^\circ$) and

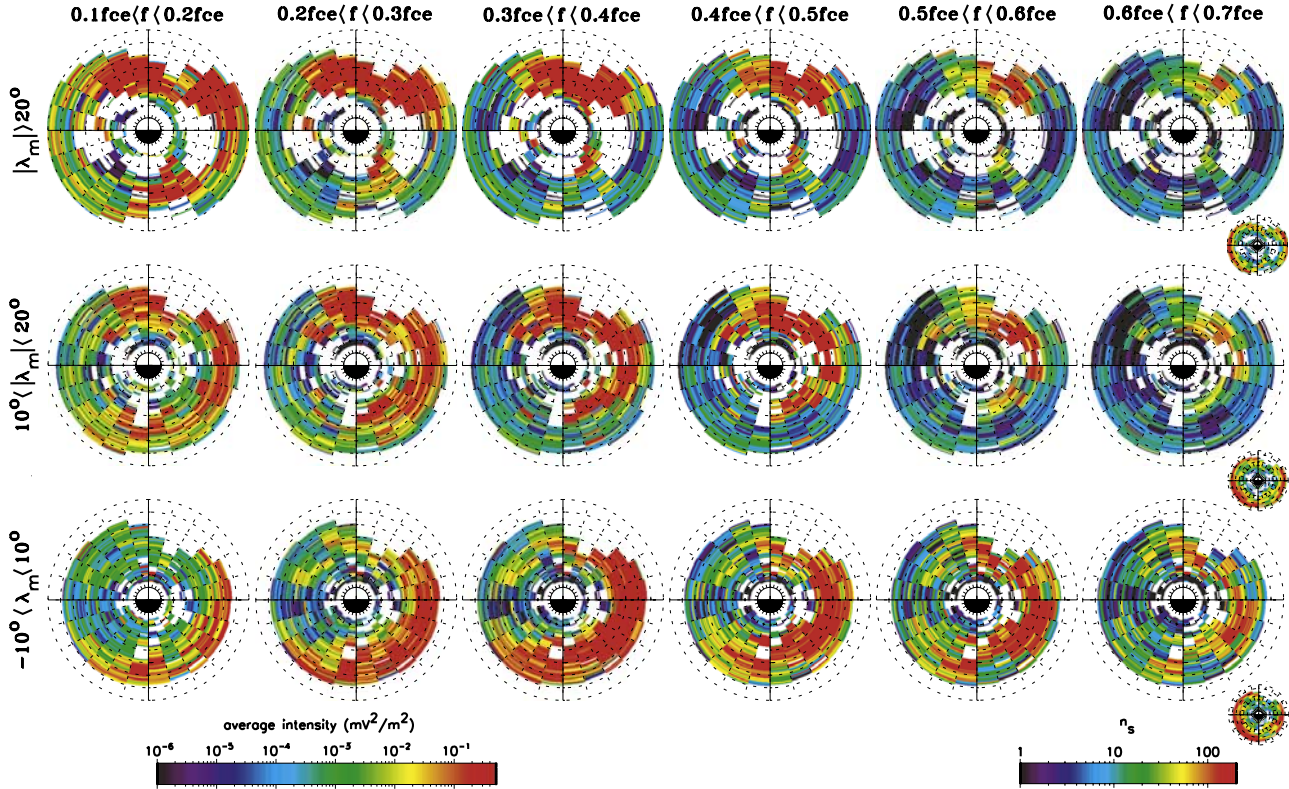


Figure 6. Distribution of chorus wave power for active conditions ($\text{AE} > 300 \text{ nT}$) as a function of L -shell and MLT, parameterized by magnetic latitude range, rows 1–3: $|\lambda_m| < 10^\circ$, $10^\circ < |\lambda_m| < 20^\circ$, $|\lambda_m| > 20^\circ$; and frequency band, normalized to the equatorial electron cyclotron frequency, columns 1–6: $f/f_{\text{ce}} = 0.1\text{--}0.2$, $0.2\text{--}0.3$, $0.3\text{--}0.4$, $0.4\text{--}0.5$, $0.5\text{--}0.6$, and $0.6\text{--}0.7$. The colorbars represent average wave intensity and number of samples in each bin.

geomagnetic activity (columns 1–3: $\text{AE} < 100 \text{ nT}$, $100 < \text{AE} < 300 \text{ nT}$, and $\text{AE} > 300 \text{ nT}$). The two lowest frequency components are shown, since these are expected to experience the least amount of damping (c.f., Figure 4). The 9 panels on the left correspond to the frequency range $0.1 f_{\text{ce}} < f < 0.2 f_{\text{ce}}$ and the 9 on the right to $0.2 f_{\text{ce}} < f < 0.3 f_{\text{ce}}$, with a dashed line showing the separation.

[31] Immediately evident is the strong degree of geomagnetic control of chorus intensity. During active times (column 3), the chorus wave power is ~ 1000 times stronger than during quiet times (column 1), since the energetic particles that drive chorus emissions ($E \sim 10\text{--}100 \text{ keV}$) are only injected when strong convection electric fields are present during active conditions [Smith *et al.*, 1999, 2004; Collier and Hughes, 2004a, 2004b]. The MLT dependence during quiet times is weak, in agreement with our theoretical predictions. During active times, there is a pronounced MLT dependence: at low latitudes, mid-latitudes, and high latitudes the chorus wave power is observed predominantly at $\text{MLT}_{\text{low}\lambda} \sim 2300\text{--}0800$, $\text{MLT}_{\text{mid}\lambda} \sim 0100\text{--}1400$, and $\text{MLT}_{\text{high}\lambda} \sim 0700\text{--}1500$ respectively (for $0.2 f_{\text{ce}} < f < 0.3 f_{\text{ce}}$). There is a clear tendency of the wave power to progressively shift to high latitudes as MLT is increased, in direct agreement with our ‘active time’ calculations (Figure 4, column c). Beyond $\text{MLT} \sim 1500$ the chorus power abruptly drops off, presumably due to the loss of the energetic electrons which are the source of the waves.

4.2. Storm-Time Chorus Distributions

[32] In Figure 6 we show the distribution of chorus wave power for active conditions (i.e., column 3 of Figure 4, $\text{AE} > 300 \text{ nT}$), parameterized by magnetic latitude range (rows 1–3: $|\lambda_m| > 20^\circ$, $10^\circ < |\lambda_m| < 20^\circ$, $|\lambda_m| < 10^\circ$) and frequency band, normalized to the equatorial electron cyclotron frequency (columns 1–6: $f/f_{\text{ce}} = 0.1\text{--}0.2$, $0.2\text{--}0.3$, $0.3\text{--}0.4$, $0.4\text{--}0.5$, $0.5\text{--}0.6$, and $0.6\text{--}0.7$).

[33] The tendency of chorus wave power to move to higher latitudes with increasing MLT is clearly evident at all frequency ranges, in agreement with our calculations. In addition, if we contrast a low frequency component (e.g., column 2, $0.2 f_{\text{ce}} < f < 0.3 f_{\text{ce}}$), with a high frequency component (e.g., column 5, $0.5 f_{\text{ce}} < f < 0.6 f_{\text{ce}}$), it is clear that significantly less power is able to propagate to high latitudes when the frequency is high, compared to when the frequency is low. This supports our theoretical prediction that Landau damping controls the latitude to which chorus waves are able to propagate, indicating larger damping at higher frequencies.

[34] By studying the L -shell distribution of the wave power, for example row 2, columns 4–6, it is apparent that the chorus wave power is able to propagate to higher latitudes at lower L -shells, in accordance with our prediction. We note that the ability to observe this L -shell distribution is also consistent with our model, and should only be evident above $f \sim 0.5 f_{\text{ce}}$ where λ_f falls in the range

10° – 20° (c.f., Figure 4), whereas lower frequency components have $\lambda_f > 20^\circ$ for most of the L -shells under study, which all fall into the highest latitude bin observed by CRRES. The fact that chorus wave power is observed only outside of $L \sim 3$ is attributed to the location of the plasmapause.

5. Discussion

[35] In the foregoing comparison, it was demonstrated that many of the observed characteristics of the chorus wave-power distribution could be successfully explained on the basis of Landau damping by the suprathermal electron (~ 1 keV) population. In particular, the tendency of lower frequency components to propagate to higher latitudes than higher frequency components was clearly shown in both our simulations and the CRRES data. The fact that chorus waves are Landau damped during their first hop away from the equator (unidirectional propagation) support previous theoretical [Bortnik et al., 2006] and observational [LeDocq et al., 1998; Lauben et al., 2002] studies (although a few observations of weak, magnetospherically reflected chorus have been made [Maeda and Smith, 1981; Parrot et al., 2003, 2004]), and the approximate final latitude to which various frequencies propagated was consistent with the CRRES data. The tendency of chorus waves to propagate to larger λ_f at lower L -shells was predicted in our simulations and observed in the CRRES data.

[36] Of particular interest was the agreement in the MLT distribution of chorus wave power, as observed at various latitudinal ranges. In both our theoretical predictions and CRRES data it was shown that chorus waves tend to be more confined to low latitudes on the nightside. The accessible latitude range of chorus increases with MLT, and peaks on the dayside. This propagation characteristic was attributed purely to the behavior of the suprathermal flux distribution.

[37] In Figure 7 the controlling influence of the suprathermal electron distribution upon wave propagation is demonstrated, by plotting the fitted flux distribution equation (1) at $L = 4.85$ as a function of MLT and E (Figure 7e), where the region $MLT = 1000$ – 1100 corresponds to incomplete CRRES coverage. The ray paths (plotted from initiation to their respective termination points) at 4 selected MLT locations are shown in Figures 7a–7d, corresponding to $MLT = 3.5, 9.5, 15.5$ and 21.5 respectively. The flux fitting parameters J_0 and m equation (1) are shown in Figures 7f and 7g and the corresponding phase space density fitting parameters A_N and n are shown in Figures 7h–7i.

[38] Figures 7e shows that $J(E)$ varies strongly as a function of MLT. When $J(E)$ is most intense, Landau damping is the most severe and propagation latitudes are the shortest (Figures 7a). As MLT increases, $J(E)$ is decreased due to scattering and loss by a number of plasma waves (including chorus) [Korth et al., 1999; Horne et al., 2003; Chen et al., 2005] and propagation lengths increase (Figures 7b), reaching a maximum at postnoon MLT (Figures 7c). Thereafter, $J(E)$ again increases towards the nightside with corresponding increase in damping (Figures 7d).

[39] Our interpretation of the flux decrease is illustrated schematically in Figures 7j, which shows the convective injection of suprathermal electrons from the plasmasheet, followed by a combination of gradient-curvature, and $\mathbf{E} \times \mathbf{B}$ drift which causes the electrons to drift in an eastward direction around the Earth. During their drift trajectories, the electrons experience scattering by a variety of plasma waves which cause losses on a timescale comparable to the strong diffusion lifetime [Horne and Thorne, 2000; Glauert and Horne, 2005] which is shorter than the drift period of the electrons, and hence the suprathermal electron population is not able to complete a full drift around the Earth (on average). Moreover, by examining Figures 7f and 7g (or alternatively Figures 7h and 7i), it is clear that not only the absolute value of the flux, J_0 , is decreased, but the spectrum becomes steeper since m progressively increases with MLT. This indicates that electrons with $E < 1$ keV and $E > 1$ keV experience different scattering rates relative to their drift timescales, with the higher energy electrons being scattered faster than the lower energy electrons. The steepening of the spectrum $J(E)$ slightly increases damping rates with MLT, but is dominated by the decrease in J_0 which drives damping rates to very low values. The tendency of lower energy electrons to propagate further in MLT is shown schematically in Figures 7j.

[40] Even though many propagation characteristics of chorus are successfully reproduced by our model, there are a few limitations which warrant discussion. Firstly, in all our simulations only the relative power of each ray was considered (Figure 3b), which implicitly assumes a uniform source of chorus waves, and neglects any inherent MLT variation in the source. This difference becomes apparent in comparing our simulation (e.g., Figure 4, panel Bc, $L > 5$) with the observations (e.g., Figure 6, column 3) where it is clear that chorus wave power drops off dramatically beyond $MLT \sim 1500$, whereas the simulations show that λ_f continues to increase until $MLT \sim 1800$. This difference is attributed to the fact that the flux of electrons responsible for the generation of chorus $E \sim 10$ – 100 keV is not uniformly distributed in MLT, but also drifts around the Earth and is scattered by various waves, decreasing both its absolute flux levels, as well as decreasing the anisotropy in the pitch-angle distribution which is presumably the source of free-energy that creates the chorus waves [Burton, 1976]. By the time the source electrons reach $MLT \sim 1500$ there is insufficient flux and anisotropy to drive chorus generation and the wave power drops off dramatically, even though propagation lengths remain high, implying that if there were any chorus waves being generated, they would have propagated to large latitudes.

[41] Secondly, in our simulations we have assumed that chorus waves are generated in a field-aligned $\psi = 0^\circ$ direction, due to the fact that cyclotron growth rates are maximized, and Landau damping rates are minimized in this configuration [Kennel, 1966; Brinca, 1972]. In addition, many observational studies have indicated that chorus is indeed observed to be predominantly field-aligned near its source [Burton and Holzer, 1974; Goldstein and Tsurutani, 1984]. While there is evidence of whistler wave-power leaking into a spectrum of non-zero wave normal angles [Lauben et al., 2002; Chum and Santolik, 2005; Santolik et al., 2006; Platino et al., 2006], it appears that the bulk of the

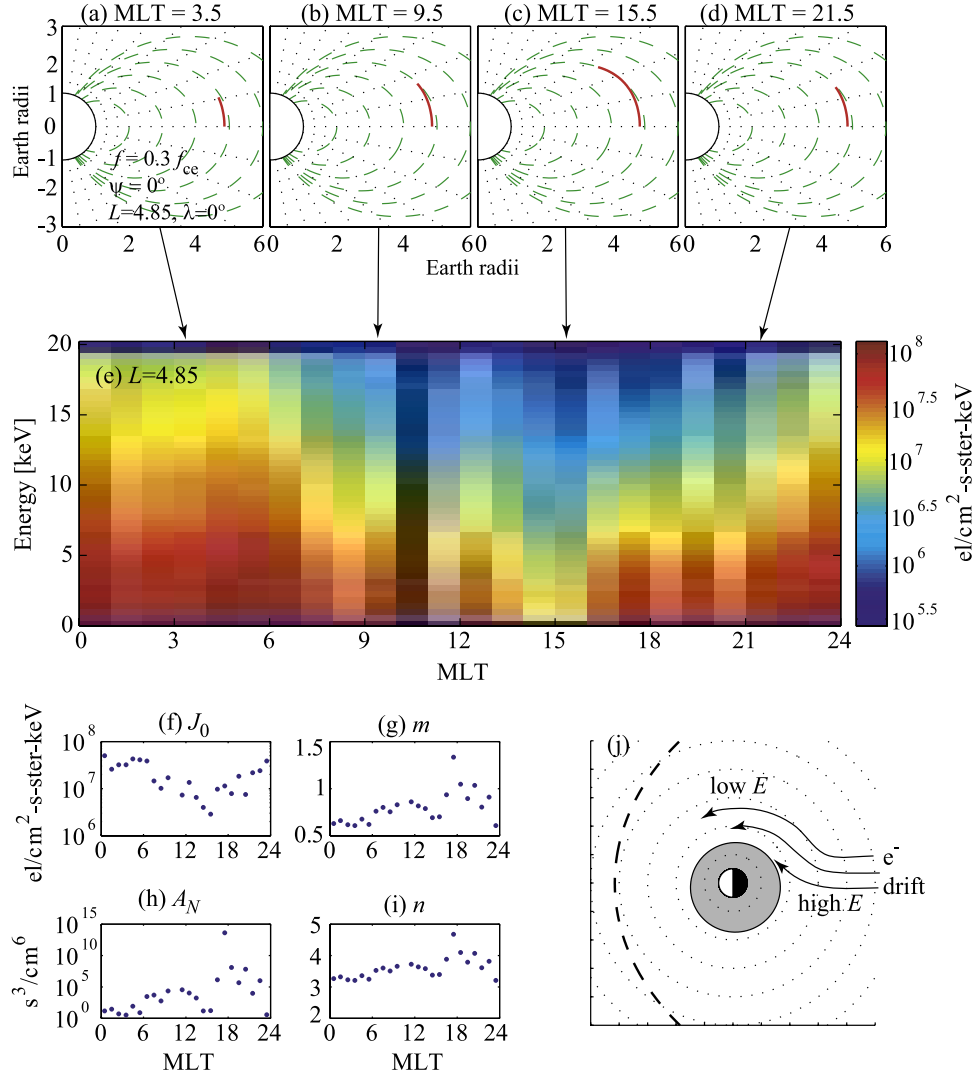


Figure 7. Suprathermal fluxes; (a)–(d) ray paths calculated at $L = 4.85$, $f = 0.3 f_{ce}$, at 4 selected MLT regions as shown; (e) suprathermal flux at $L = 4.85$ as a function of MLT and energy; (f) fitted parameters for flux distribution J_0 , and (g) m ; (h) fitted parameters for phase space density distribution, A_N and (i), all shown as a function of MLT.

wave power is indeed initiated in a field-aligned orientation, and the observed large-scale characteristics reported in this paper are consistent with this generation regime.

[42] Finally, we note that in our simulation we have assumed that chorus waves are instantaneously produced at the geomagnetic equator and then propagate away, which is an overly simplistic treatment of the chorus generation problem [a very complicated problem indeed! e.g., *Helliwell*, 1967, 1995; *Omura et al.*, 1991; *Hattori et al.*, 1991; *Sazhin and Hayakawa*, 1992; *Trakhtengerts*, 1995, 1999; *Nunn et al.*, 1997]. An example of source dynamics can be seen in Figure 6, e.g., columns 1 and 2, where the chorus wave power is seen to be relatively weak on the dayside at $|\lambda_m| < 10^\circ$, and increases with latitude, reaching a maximum at $|\lambda_m| > 20^\circ$. This distribution of wave power has led some authors to suggest that the chorus generation region could be located at high latitudes on the dayside [*Tsurutani and Smith*, 1977] but recent studies of Poynting flux show that even though wave power maximises at high latitudes on the

dayside, the propagation direction is uniformly away from the equator at all MLT [*LeDocq et al.*, 1998; *Lauben et al.*, 2002; *Santolik et al.*, 2004, 2005]. A possible interpretation of this behavior based on quasilinear theory, is that the cyclotron growth rates responsible for the generation of chorus become progressively lower with increasing MLT, due to the scattering (loss) and isotropization of the source population of electrons $E \sim 10\text{--}100$ keV. To reach a given amplitude (in order to reach the nonlinear threshold), the chorus waves need to propagate for a longer distance due to the lower cyclotron growth rate, which is made possible by the concomitant decrease in the Landau fluxes and resultant increase in λ_f (Figure 4), as well as decreased field-line inhomogeneity on the dayside [*Tsyganenko and Sitnov*, 2005] allowing more uniform wave propagation. The above interpretation is consistent with the fact that it is predominantly the lower frequency waves which show the extended growth region. Since lower frequency waves resonate with higher energy electrons, which are far less numerous than

lower energy electrons, it is the lower frequencies which will have the lowest growth rates and hence require the largest propagation distance to achieve significant total amplification. Wave power density increase is also enhanced due to magnetic field line convergence at high latitudes.

6. Conclusions

[43] In the present paper, statistical distributions of suprathermal electrons ($E = 0.213\text{--}16.5$ keV) from the CRRES satellite were used to fit analytical phase space density distributions of the form $f(v) = A_N/v^n$, as a function of L -shell, MLT, and geomagnetic activity. These fitted distributions were then used in conjunction with ray tracing to calculate the Landau damping rates of an ensemble of rays representing chorus waves. The modeled propagation characteristics were compared to statistical observations of chorus wave power, also from the CRRES satellite, in various frequency bands ($f/f_{ce} = 0.1\text{--}0.2, 0.2\text{--}0.3, \dots, 0.6\text{--}0.7$), latitude ranges ($|\lambda_m| < 10^\circ, 10^\circ < |\lambda_m| < 20^\circ$, and $|\lambda_m| < 20^\circ$), and under a variety of geomagnetic conditions ($AE < 100$ nT, $100 < AE < 300$ nT, and $AE > 300$ nT).

[44] Based on the work presented in this paper, a number of conclusions can be drawn:

[45] 1. At all wave frequencies and geomagnetic activity conditions, chorus rays were Landau damped before they were able to magnetospherically reflect, consistent with the observed unidirectional propagation observed generally away from the equator.

[46] 2. Chorus rays propagated to larger latitudes at lower L -shells (but outside the plasmapause) than at larger L -shells, due to the lower ratio of N_h/N_0 (number of ‘hot’ electrons relative to the cold background electron number density).

[47] 3. Lower frequency rays were found to propagate to higher latitudes than higher frequency rays, consistent with CRRES observations. In addition, there was good agreement between the absolute value of the final latitudes predicted by our model and the inferred final latitude from the CRRES observations.

[48] 4. The MLT distribution of chorus wave power was found to be relatively uniform or unstructured during geomagnetically quiet conditions, but showed a pronounced asymmetry during active conditions, with small propagation latitudes on the nightside, and large propagation latitudes on the dayside. This asymmetry was well reflected in the CRRES observations.

[49] 5. The MLT distributions of chorus wave power under active conditions were found to be strongly controlled by the underlying distribution of suprathermal electrons, which were most intense on the nightside resulting in the most severe damping, and gradually decayed towards the dayside where large propagation lengths were observed. This depletion of suprathermal particles was interpreted on the basis of the loss timescales being faster than drift timescales, with the higher energy particles being affected more than the lower energy electrons.

[50] It was shown that many characteristics of the chorus wave-power distribution in L , MLT, and latitude, were explained very well on the basis of Landau damping by the suprathermal particle population. This important population of particles may thus be indirectly responsible for controlling the dynamics of the relativistic radiation-belt

electrons, since many of the theories of chorus acceleration and loss rely on the interaction between chorus waves and energetic particles at mid- and high- latitudes [Horne et al., 2005b; Thorne et al., 2005a, 2005b].

[51] It was also shown that certain features appear in the chorus wave distribution on the dayside, which are almost certainly related to the dynamics of the energetic electrons $E \sim 10\text{--}100$ keV responsible for the generation of the chorus waves. Although we have proposed a preliminary reason for this behavior, it remains to be treated in a more quantitative way in future studies.

[52] **Acknowledgments.** JB and RMT would like to acknowledge support from NSF grants ATM-0402615 and ATM-0621724 (GEM postdoc award), as well as NASA grants NNG04GM44G and NNG04-G01G through subcontract 17496790-30026-A with Stanford University. NPM would like to acknowledge support from the Natural Environment Research Council, U.K. The authors would like to thank Roger R. Anderson for provision of the CRRES plasma wave data used in this study, and Richard B. Horne for useful discussion. We also thank NSSDC Omniweb for providing the geomagnetic index data used in the paper.

[53] Zuyin Pu thanks Ondrej Santolik and Geoffrey Reeves for their assistance in evaluating this paper.

References

- Abel, G. A., M. P. Freeman, A. J. Smith, and G. D. Reeves (2006), Association of substorm chorus events with drift echos, *J. Geophys. Res.*, **111**, A11220, doi:10.1029/2006JA011860.
- Anderson, R. R., and K. Maeda (1977), VLF emissions associated with enhanced magnetospheric electrons, *J. Geophys. Res.*, **82**, 135–146.
- Anderson, R. R., D. A. Gurnett, and D. L. Odem (1992), CRRES plasma wave experiment, *J. Spacecr. Rockets*, **29**, 570.
- Angerami, J. J., and J. O. Thomas (1964), Studies of planetary atmospheres. I. Distribution of electrons + ions in Earth’s exosphere, *J. Geophys. Res.*, **69**(21), 4537.
- Asnes, A., J. Stadsnes, R. W. Friedel, N. Ostgaard, and M. Thomsen (2005), Medium energy pitch angle distribution during substorm injected electron clouds, *Geophys. Res. Lett.*, **32**, L10101, doi:10.1029/2004GL022008.
- Bell, T. F., U. S. Inan, J. Bortnik, and J. D. Scudder (2002), The Landau damping of magnetospherically reflected whistlers within the plasma sphere, *Geophys. Res. Lett.*, **29**(15), 1733, doi:10.1029/2002GL014752.
- Bortnik, J., and R. M. Thorne (2006), The dual role of ELF/VLF chorus waves in the acceleration and precipitation of radiation belt electrons, *J. Atmos. Sol. Terr. Phys.*, [in print].
- Bortnik, J., U. S. Inan, and T. F. Bell (2003), Energy distribution and lifetime of magnetospherically reflecting whistlers in the plasmasphere, *J. Geophys. Res.*, **108**(A5), 1199, doi:10.1029/2002JA009316.
- Bortnik, J., U. S. Inan, and T. F. Bell (2006), Landau damping and resultant unidirectional propagation of chorus waves, *Geophys. Res. Lett.*, **33**, L03102, doi:10.1029/2005GL024553.
- Brinca, A. L. (1972), On the stability of obliquely propagating whistlers, *J. Geophys. Res.*, **77**(19), 3495.
- Burtis, W. J., and R. A. Helliwell (1969), Banded chorus — a new type of VLF radiation observed in the magnetosphere by OGO 1 and OGO 3, *J. Geophys. Res.*, **74**, 3002.
- Burtis, W. J., and R. A. Helliwell (1976), Magnetospheric chorus: Occurrence patterns and normalized frequency, *Planet. Space Sci.*, **24**(11), 1007–1023.
- Burton, R. K. (1976), Critical electron pitch angle anisotropy necessary for chorus generation, *J. Geophys. Res.*, **81**, 4779–4781.
- Burton, R. K., and R. E. Holzer (1974), The origin and propagation of chorus in the outer magnetosphere, *J. Geophys. Res.*, **79**(7), 1014–1023.
- Carpenter, D. L., and R. R. Anderson (1992), An ISEE/Whistler Model of Equatorial electron-density in the magnetosphere, *J. Geophys. Res.-Space Phys.*, **97**(A2), 1097–1108.
- Chen, M. W., M. Schulz, P. C. Anderson, G. Lu, G. Germany, and M. Wüest (2005), Storm time distributions of diffuse auroral electron energy and X-ray flux: Comparison of drift-loss simulations with observations, *J. Geophys. Res.*, **110**, A03210, doi:10.1029/2004JA010725.
- Chum, J., and O. Santolik (2005), Propagation of whistler-mode chorus to low altitudes: divergent ray trajectories and ground accessibility, *Annales Geophysicae*, **23**(12), 3727–3738.
- Collier, A., and A. Hughes (2004a), Modeling substorm chorus events in terms of dispersive azimuthal drift, *Ann. Geophys.*, **22**(12), 4311–4327.
- Collier, A., and A. R. W. Hughes (2004b), Modeling and analysis of substorm related chorus events, *Adv. Space Res.*, **34**(8), 1819–1823.

- Glauert, S. A., and R. B. Horne (2005), Calculation of pitch angle and energy diffusion coefficients with the PADIE code, *J. Geophys. Res.*, **110**, A04206, doi:10.1029/2004JA010851.
- Goldstein, B. E., and B. T. Tsurutani (1984), Wave normal directions of chorus near the equatorial source region, *J. Geophys. Res.*, **89**(A5), 2789–2810.
- Hardy, D. A., D. M. Walton, A. D. Johnstone, M. F. Smith, M. P. Gough, A. Huber, J. Pantazis, and R. Burkhardt (1993), Low energy plasma analyser, *IEEE Trans. Nucl. Sci.*, **40**, 246.
- Hattori, K., M. Hayakawa, D. Lagoutte, M. Parrot, and F. Lafeuvre (1991), Further evidence of triggering chorus emissions from the wavelets in the hiss band, *Planet. and Space Sci.*, **39**(11), 1465–1472.
- Helliwell, R. A. (1965), *Whistlers and related ionospheric phenomena*, Stanford University Press, Stanford, Calif.
- Helliwell, R. A. (1967), A Theory of Discrete VLF Emissions from Magnetosphere, *J. Geophys. Res.*, **72**(19), 4773–4790.
- Helliwell, R. A. (1995), The role of the Gendrin mode of VLF propagation in the generation of magnetospheric emissions, *Geophys. Res. Lett.*, **22**(16), 2095–2098, doi:10.1029/95GL02003.
- Horne, R. B., and R. M. Thorne (1998), Potential waves for relativistic electron scattering and stochastic acceleration during magnetic storms, *Geophys. Res. Lett.*, **25**, 3011.
- Horne, R. B., and R. M. Thorne (2000), Electron pitch angle diffusion by electrostatic electron cyclotron harmonic waves: the origin of pancake distributions, *J. Geophys. Res.*, **105**(A3), 5391–5402, doi:10.1029/1999JA90447.
- Horne, R. B., and R. M. Thorne (2003), Relativistic electron acceleration and precipitation during resonant interactions with whistler mode chorus, *Geophys. Res. Lett.*, **30**(10), 1527, doi:10.1029/2003GL016973.
- Horne, R. B., N. P. Meredith, R. M. Thorne, D. Heynderickx, R. H. A. Iles, and R. R. Anderson (2003), Evolution of energetic electron pitch angle distributions during storm time electron acceleration to megaelectronvolt energies, *J. Geophys. Res.*, **108**(A1), 1016, doi:10.1029/2001JA009165.
- Horne, R. B., et al. (2005a), Wave acceleration of electrons in the Van Allen radiation belts, *Nature*, **437**(7056), 227–230, doi:10.1038/nature03939.
- Horne, R. B., R. M. Thorne, S. A. Glauert, J. M. Albert, N. P. Meredith, and R. R. Anderson (2005b), Timescale for radiation belt electron acceleration by whistler mode chorus waves, *J. Geophys. Res.*, **110**, A03225, doi:10.1029/2004JA010811.
- Horne, R. B., N. P. Meredith, S. A. Glauert, A. Varotsou, R. M. Thorne, Y. Y. Shprits, and R. R. Anderson (2006), Mechanisms for the acceleration of radiation belt electrons, in *Recurrent Magnetic Storms: Corotating Solar Wind Streams*, *Geophys. Monogr. Ser.*, vol. 167, edited by B. T. Tsurutani, R. L. McPherron, W. D. Gonzalez, G. Lu, J. H. Sobral, and N. Gopalswamy, pp 151–173, AGU, Washington, D. C.
- Inan, U. S., and T. F. Bell (1977), The Plasmapause as a VLF Wave Guide, *J. Geophys. Res.*, **82**(19), 2819–2827.
- Johnson, M. H., and J. Kierein (1992), Combined release and radiation effects satellite (CRRES) — spacecraft and mission, *Journal of Spacecraft and Rockets*, **29**(4), 556–563.
- Kennel, C. (1966), Low-frequency whistler mode, *Phys. Fluids*, **9**(11).
- Kennel, C. F., and R. M. Thorne (1967), Unstable growth of unducted whistlers propagating at an angle to the geomagnetic field, *J. Geophys. Res.*, **72**, 871.
- Kirkpatrick, S., C. D. Gelatt Jr., and M. P. Vecchi (1983), Optimization by simulated annealing, *Science*, **220**(4598).
- Kondrashov, D., and M. Ghil (2006), Spatio-temporal filling of missing data points in geophysical data sets, *Nonlin. Processes Geophys.*, **13**, 151–159.
- Koons, H. C., and J. L. Roeder (1990), A survey of equatorial magnetospheric wave activity between 5 and 8 R_E , *Planet. Space Sci.*, **38**(10), 1335–1341.
- Korth, H., M. F. Thomsen, J. E. Borovsky, and D. J. McComas (1999), Plasma sheet access to geosynchronous orbit, *J. Geophys. Res.*, **104**(A11), 25,047–25,061.
- Lauben, D. S., U. S. Inan, T. F. Bell, and D. A. Gurnett (2002), Source characteristics of ELF/VLF chorus, *J. Geophys. Res.*, **107**(A12), 1429, doi:10.1029/2000JA003019.
- LeDucq, M. J., D. A. Gurnett, and G. B. Hospodarsky (1998), Chorus source locations from VLF Poynting flux measurements with the Polar spacecraft, *Geophys. Res. Lett.*, **25**(21), 4063–4066.
- Lubchich, A. A., A. G. Yahnin, E. E. Titova, A. G. Demekhov, V. Yu. Trakhtengerts, J. Manninen, and T. Turunen (2006), Longitudinal drift of substorm electrons as the reason of impulsive precipitation events and VLF emissions, *Annales Geophysicae*, **24**, 2667–2684.
- Lyons, L. R., D.-Y. Lee, R. M. Thorne, R. B. Horne, and A. J. Smith (2005), Solar wind-magnetosphere coupling leading to relativistic electron energization during high-speed streams, *J. Geophys. Res.*, **110**, A11202, doi:10.1029/2005JA011254.
- Maeda, K., and P. H. Smith (1981), VLF emissions associated with ring current electrons: off equatorial observations, *Planet. Space Sci.*, **29**(8), 825–835.
- Meredith, N. P., R. B. Horne, and R. R. Anderson (2001), Substorm dependence of chorus amplitudes: Implications for the acceleration of electrons to relativistic energies, *J. Geophys. Res.*, **106**(A7), 13,165–13,178.
- Meredith, N. P., R. B. Horne, D. Summers, R. M. Thorne, R. H. A. Iles, D. Heynderickx, and R. R. Anderson (2002a), Evidence for acceleration of outer zone electrons to relativistic energies by whistler mode chorus, *Ann. Geophys.*, **20**, 967.
- Meredith, N. P., R. B. Horne, R. H. A. Iles, R. M. Thorne, D. Heynderickx, and R. R. Anderson (2002b), Outer zone relativistic electron acceleration associated with substorm-enhanced whistler mode chorus, *J. Geophys. Res.*, **107**(A7), 1144, doi:10.1029/2001JA900146.
- Meredith, N. P., R. B. Horne, R. M. Thorne, and R. R. Anderson (2003a), Favored regions for chorus-driven electron acceleration to relativistic energies in the Earth's outer radiation belt, *Geophys. Res. Lett.*, **30**(16), 1871, doi:10.1029/2003GL017698.
- Meredith, N. P., M. Cain, R. B. Horne, R. M. Thorne, D. Summers, and R. R. Anderson (2003b), Evidence for chorus-driven electron acceleration to relativistic energies from a survey of geomagnetically disturbed periods, *J. Geophys. Res.*, **108**(A6), 1248, doi:10.1029/2002JA009764.
- Meredith, N. P., R. B. Horne, R. M. Thorne, D. Summers, and R. R. Anderson (2004), Substorm dependence of plasmaspheric hiss, *J. Geophys. Res.*, **109**, A06209, doi:10.1029/2004JA010387.
- Miyoshi, Y., A. Morioka, H. Misawa, T. Obara, T. Nagai, and Y. Kasahara (2003), Rebuilding process of the outer radiation belt during the 3 November 1993 magnetic storm: NOAA and Exos-D observations, *J. Geophys. Res.*, **108**(A1), 1004, doi:10.1029/2001JA007542.
- Nunn, D., Y. Omura, H. Matsumoto, I. Nagano, and S. Yagitani (1997), The numerical simulation of VLF chorus and discrete emissions observed on the Geotail satellite using a Vlasov code, *J. Geophys. Res.*, **102**(A12), 27,083–27,098.
- Omura, Y., D. Nunn, H. Matsumoto, and M. J. Rycroft (1991), A review of observational, theoretical, and numerical studies of VLF triggered emissions, *J. Atmos. Terr. Phys.*, **53**, 351–368.
- Parrot, M., O. Santolik, N. Cornilleau-Wehrlin, M. Maksimovic, and C. Harvey (2003), Magnetospherically reflected chorus waves revealed by ray tracing with CLUSTER data, *Ann. Geophys.*, **21**(5), 1111–1120.
- Parrot, M., O. Santolik, D. Gurnett, J. Pickett, and N. Cornilleau-Wehrlin (2004), Characteristics of magnetospherically reflected chorus waves observed by CLUSTER, *Ann. Geophys.*, **22**(7), 2597–2606.
- Platino, M., U. S. Inan, T. F. Bell, J. S. Pickett, and P. Canu (2006), Rapidly moving sources of upper band ELF/VLF chorus near the magnetic equator, *J. Geophys. Res.*, **111**, A09218, doi:10.1029/2006JA011468.
- Press, W. H., S. A. Teukolsky, W. T. Vetterling, and B. P. Flannery (2002), *Numerical Recipes in C*, Cambridge University Press.
- Santolik, O., and D. A. Gurnett (1965), Transverse dimensions of chorus in the source region, *Geophys. Res. Lett.*, **30**(2), 1–3, 1031, doi:10.1029/2002GL016178.
- Santolik, O., D. A. Gurnett, J. S. Pickett, M. Parrot, and N. Cornilleau-Wehrlin (2003), Spatio-temporal structure of storm-time chorus, *J. Geophys. Res.*, **108**(A7), 1278, doi:10.1029/2002JA009791.
- Santolik, O., D. A. Gurnett, and J. S. Pickett (2004), Multipoint investigation of the source region of storm-time chorus, *Ann. Geophys.*, **22**, 2555–2563.
- Santolik, O., D. A. Gurnett, J. S. Pickett, M. Parrot, and N. Cornilleau-Wehrlin (2005), Central position of the source region of storm-time chorus, *Planet. Space Sci.*, **53**, 299–305.
- Santolik, O., J. Chum, M. Parrot, D. A. Gurnett, J. S. Pickett, and N. Cornilleau-Wehrlin (2006), Propagation of whistler mode chorus to low altitudes: Spacecraft observations of structured ELF hiss, *J. Geophys. Res.*, **111**, A10208, doi:10.1029/2005JA011462.
- Sazhin, S. S., and M. Hayakawa (1992), Magnetospheric chorus emissions: A review, *Planet. Space Sci.*, **40**(5), 681–697.
- Shprits, Y. Y., R. M. Thorne, R. B. Horne, S. A. Glauert, M. Cartwright, C. T. Russell, D. N. Baker, and S. G. Kanekal (2006), Acceleration mechanism responsible for the formation of the new radiation belt during the 2003 Halloween solar storm, *Geophys. Res. Lett.*, **33**, L05104, doi:10.1029/2005GL024256.
- Singer, H. J., W. P. Sullivan, P. Anderson, F. Mozer, P. Harvey, J. Wygant, and W. McNeil (1992), Fluxgate magnetometer instrument on the CRRES, *J. Spacecr. Rockets*, **29**, 599.
- Smith, A. J., M. P. Freeman, M. G. Wickett, and B. D. Cox (1999), On the relationship between the magnetic and VLF signatures of the substorm expansion phase, *J. Geophys. Res.*, **104**(A6), 12,351–12,360.
- Smith, A. J., R. B. Horne, and N. P. Meredith (2004), Ground observations of chorus following geomagnetic storms, *J. Geophys. Res.*, **109**, A02205, doi:10.1029/2003JA010204.

- Spasojevic, M., and U. S. Inan (2005), Ground based VLF observations near $L = 2.5$ during the Halloween 2003 storm, *Geophys. Res. Lett.*, **32**, L21103, doi:10.1029/2005GL024377.
- Storey, L. R. O. (1953), An investigation of whistling atmospherics, *Phil. Trans. Roy. Soc.*, **246**(908), 113–141.
- Summers, D., R. M. Thorne, and F. Xiao (1998), Relativistic theory of wave-particle resonant diffusion with application to electron acceleration in the magnetosphere, *J. Geophys. Res.*, **103**, 20,487–20,500.
- Summers, D., C. Ma, N. P. Meredith, R. B. Horne, R. M. Thorne, and R. R. Anderson (2004), Modeling outer-zone relativistic electron response to whistler-mode chorus activity during substorms, *J. Atmos. Sol. Terr. Phys.*, **66**(2), 133–146.
- Thorne, R. M., and R. B. Horne (1994), Landau damping of magnetospherically reflected whistlers, *J. Geophys. Res. Space Phys.*, **99**(A9), 17,249–17,258.
- Thorne, R. M., and C. F. Kennel (1967), Quasi-trapped VLF propagation in the outer magnetosphere, *J. Geophys. Res.*, **72**, 857–870.
- Thorne, R. M., T. P. O'Brien, Y. Y. Shprits, D. Summers, and R. B. Horne (2005a), Timescale for MeV electron microburst loss during geomagnetic storms, *J. Geophys. Res.*, **110**, A09202, doi:10.1029/2004JA010882.
- Thorne, R. M., R. B. Horne, S. A. Glauert, N. P. Meredith, Y. Y. Shprits, D. Summers, and R. R. Anderson (2005b), The influence of wave-particle interactions on relativistic electron dynamics during storms, in *Inner Magnetosphere Interactions: New Perspectives from Imaging*, *Geophys. Monogr. Ser.*, vol. 159, edited by J. L. Burch, M. Schulz, and H. Spence, pp 101–112, AGU, Washington, D. C.
- Trakhtengerts, V. Y. (1995), Magnetosphere cyclotron maser: backward wave oscillator generation regime, *J. Geophys. Res.*, **100**(A9), 17,205–17,210.
- Trakhtengerts, V. Y. (1999), A generation mechanism for chorus emission, *Ann. Geophys.*, **17**, 95–100.
- Tsurutani, B. T., and E. J. Smith (1974), Postmidnight chorus: A substorm phenomenon, *J. Geophys. Res.*, **79**(1), 118–127.
- Tsurutani, B. T., and E. J. Smith (1977), Two types of magnetospheric ELF chorus and their substorm dependences, *J. Geophys. Res.*, **82**, 5112–5128.
- Tsyganenko, N. A., and M. I. Sitnov (2005), Modeling the dynamics of the inner magnetosphere during strong geomagnetic storms, *J. Geophys. Res.*, **110**, A03208, doi:10.1029/2004JA010798.
- Varotsou, A., D. Boscher, S. Bourdarie, R. B. Horne, S. A. Glauert, and N. P. Meredith (2005), Simulation of the outer radiation belt electrons near geosynchronous orbit including both radial diffusion and resonant interaction with whistler mode chorus waves, *Geophys. Res. Lett.*, **32**, L19106, doi:10.1029/2005GL023282.
- Walt, M. (1994), *Introduction to geomagnetically trapped radiation*, Cambridge University Press.

J. Bortnik and R. M. Thorne, Department of Atmospheric and Oceanic Sciences, University of California, Los Angeles, CA 90095-1565, USA.
(jbortnik@gmail.com; rmt@atmos.ucla.edu)

N. P. Meredith, British Antarctic Survey, Natural Environment Research Council, Madingley Road, Cambridge, CB3 0ET, UK. (nmer@bas.ac.uk)